Journal of Molecular Modeling (2021) 27:130
https://doi.org/10.1007/s00894-021-04739-8

ORIGINAL PAPER

Cage-like La_4B_{24} and Core-Shell $La_4B_{29}^{0/+/-}$: perfect spherically aromatic tetrahedral metallo-borospherenes

Xiao-Qin Lu[1] · Cai-Yue Gao[1] · Zhihong Wei[1] · Si-Dian Li[1]

Received: 28 January 2021 / Accepted: 15 March 2021

Abstract

Cage-like and core-shell metallo-borospherenes exhibit interesting structures and bonding. Based on extensive global searches and first-principles theory calculations, we predict herein the perfect tetrahedral cage-like T_d La_4B_{24} (**1**) and core-shell T_d La_4B_{29} (**2**), T_d $La_4B_{29}^+$ (**3**), and T_d $La_4B_{29}^-$ (**4**) which all possess the same geometrical symmetry as their carbon fullerene counterpart T_d C_{28}, with four equivalent interconnected B_6 triangles on the cage surface and four nona-coordinate La centers in four conjoined η^9-B_9 rings. In these tetra-La-doped boron complexes, $La_4[B@B_4@B_{24}]^{0/+/-}$ (**2**/**3**/**4**) in the structural motif of 1 + 4 + 28 contain a B-centered tetrahedral T_d $B@B_4$ core in a La-decorated tetrahedral La_4B_{24} shell, with the negatively charged tetra-coordinate B^- at the center being the boron analog of tetrahedral C in T_d CH_4 (B^- ~ C). Detailed orbital and bonding analyses indicate that these T_d lanthanide boride complexes are spherically aromatic in nature with a universal La–B_9 (d-p) σ and (d-p) δ coordination bonding pattern. The IR, Raman, and UV-Vis or photoelectron spectra of these novel metallo-borospherenes are computationally simulated to facilitate their spectral characterizations.

Keywords First-principles theory · Metallo-Borospherenes · Tetrahedral structures · Bonding patterns · Spherical Aromaticity

Introduction

Boron as a prototypical electron-deficient element possesses a rich chemistry next only to carbon in the periodical table. It exhibits a strong propensity to form multi-center-two-electron (mc-2e) bonds in both bulk allotropes and polyhedral molecules [1, 2]. Persistent joint photoelectron spectroscopy (PES) and first-principles theory investigations in the past two decades have unveiled a rich landscape for size-selected boron clusters ($B_n^{-/0}$) from planar or quasi-planar structures (n = 3–38, 41, 42) to cage-like borospherenes (C_3/C_2 B_{39}^- and D_{2d} $B_{40}^{-/0}$) which are all characterized with delocalized multi-center bonding [2–6]. Seashell-like borospherenes C_2 B_{28}^- and C_s B_{29}^- were late observed in PES measurements as minor isomers competing with their quasi-planar global minimum (GM) counterparts [7, 8]. Endohedral M@B_{40} (M = Ca, Sr) and exohedral M&B_{40} (M = Be, Mg) metallo-borospherenes were predicted in theory shortly after the discovery of D_{2d} $B_{40}^{-/0}$ [9]. Endohedral metallo-borospherenes D_2 $Ta@B_{22}^-$ and D_{2d} U@B_{40} were proposed to be superatoms matching the 18-electron rule and 32-electron principles, respectively [10, 11]. Joint ion-mobility measurements and density functional theory (DFT) investigations indicated that boron cluster monocations (B_n^+) possess double-ring tubular geometries in the size range between n = 16–25 [12]. Extensive GM searches showed that complicated structural competitions exist in medium-sized B_n clusters, with B_{46} being the smallest core-shell boron cluster ($B_4@B_{42}$) and B_{48}, B_{54}, B_{60}, and B_{62} being the first bilayer boron clusters predicted to date [13, 14].

Transition-metal-doping induces earlier planar→tubular→cage-like→core-shell structural transitions in boron clusters, resulting in unique structures and bonding in chemistry. Typical examples include the experimentally observed transition-metal-centered boron wheels M@B_n ($Co@B_8^-$, $Ru@B_9^-$, and $Ta@B_{10}^-$) and transition-metal-centered boron drums M@B_n^- ($Mn@B_{16}^-$, $Co@B_{16}^-$, $Rh@B_{18}^-$, and $Ta@B_{20}^-$) [15–20]. A family of di-La-doped inverse-sandwich-type mono-deck boron clusters $La_2B_n^-$ (n = 7–9) [21, 22] and inverse triple-decker $La_3B_{14}^-$ were observed in PES

✉ Zhihong Wei
weizhihong@sxu.edu.cn

✉ Si-Dian Li
lisidian@sxu.edu.cn

[1] Institute of Molecular Science, University of Shanxi, Taiyuan 030006, China

Published online: 21 April 2021

experiments [23]. The first tri-La-doped spherical trihedral metallo-borospherene D_{3h} $La_3B_{18}^-$ with three La atoms as integral parts of the cage surface was discovered very recently in a joint experimental and theoretical investigation [24]. Our group predicted the possibility of the smallest inverse sandwich bi-decker tubular molecular rotor C_{2h} La_2B_{20} ($La_2[B_2@B_{18}]$) [25] and the first core-shell spherical trihedral metallo-borospherenes D_{3h} $La_3B_{20}^-$ ($La_3[B_2@B_{18}]^-$) which contains two equivalent eclipsed B_6 triangles on the top and bottom interconnected by three B_2 units on the waist and three deca-coordinate La atoms as integral parts of cage surface [26]. We also reported the smallest metallo-borospherene D_{3h} $Ta_3B_{12}^-$ composed of two eclipsed B_3 triangles on the top and bottom interconnected by three B_2 units on the waist [27]. However, to the best of our knowledge, there have been no experimental or theoretical evidence reported on tetra-La-doped boron clusters to date. Tetra-metal-doped core-shell metallosilicon fullerenes T_d $M_4@Si_{28}$ (M = Al and Ga) in the structural motif of 4 + 28 have been predicted [28] to have the same tetrahedral symmetry as their carbon fullerene counterpart T_d C_{28} [29]. It is natural to ask at current stage what geometrical structures and bonding patterns of the tetra-La-doped boron clusters may have and if perfect tetrahedral metallo-borospherenes are favored over other geometries in both thermodynamics and dynamics.

Based on extensive GM searches and first-principles theory calculations, as an extension of the experimentally observed cage-like D_{3h} $La_3B_{18}^-$ [24] and theoretically predicted core-shell D_{3h} $La_3B_{20}^-$ [25], we predict herein the perfect tetrahedral cage-like T_d La_4B_{24} (**1**) and core-shell T_d La_4B_{29} (**2**), T_d $La_4B_{29}^+$ (**3**), and T_d $La_4B_{29}^-$ (**4**) which possess four equivalent inter-connected B_6 triangles on the cage surface and four nona-coordinate La centers in four equivalent conjoined η^9-B_9 nonagonal ligands, presenting the first metallo-borobspherene counterparts of the experimentally observed tetrahedral carbon fullerene T_d C_{28} [29]. More intriguingly, $La_4[B@B_4@B_{24}]^{0/+/-}$ (**2/3/4**) in the structural pattern of 1 + 4 + 28 possess a tetra-coordinate B center encapsulated in an inner tetrahedron $(B^i)_4$ and an outer tetrahedron $La_4(B^o)_{24}$. These high-symmetry lanthanide boride complexes turn out to be spherically aromatic in nature with a universal La–B_9 (p-d) σ and (p-d) δ coordination bonding pattern.

Methods

Extensive GM searches were performed on La_4B_{24}, $La_4B_{29}^+$ and $La_4B_{29}^-$ using the TGmin2 code [30] at DFT level, with the initial seeds being manually constructed based on the experimentally observed $La_3B_{18}^-$ [24] and theoretically predicted $La_3B_{19}^-$ and $La_3B_{20}^-$ [26]. Over 2000 trial structures were explored for each species in both singlet and triplet states at PBE/TZVP. The low-lying isomers were subsequently optimized at the PBE0 [31] and TPSSh [32] levels with the basis set of 6–311 + G(d) [33] for B and Stuttgart relativistic small-core pseudopotential for La [34, 35] using the Gaussian 09 program suite [36], with the vibrational frequencies checked to make sure all the obtained structures are true minima on the potential surfaces. Low-lying isomers of the open-shell neutral La_4B_{29} were acquired from the corresponding low-lying isomers of $La_4B_{29}^+$ and $La_4B_{29}^-$. Relative energies of the three lowest-lying isomers were further refined for La_4B_{24} and $La_4B_{29}^+$ at the coupled cluster CCSD(T)/6-31G(d) level [37–39] implemented in MOLPRO [40] at PBE0 geometries. Chemical bonding analyses were performed for La_4B_{24} (**1**) and $La_4[B@B_4@B_{24}]^+$ (**3**) using the adaptive natural density partitioning (AdNDP) approach [41] at the PBE0 level. Natural bonding orbital (NBO) analyses were achieved using the NBO 6.0 program [42]. Born–Oppenheimer molecular dynamics (BOMD) simulations were carried out on La_4B_{24} (**1**), La_4B_{29} (**2**), $La_4B_{29}^+$ (**3**), and $La_4B_{29}^-$ (**4**) for 30 ps at 300 K and 1000 K using the CP2K code [43].

Results and discussion

Strucutres and stabilities

With inspiration from the previously reported D_{3h} $La_3B_{18}^-$ and D_{3h} $La_3B_{20}^-$ [24, 26] which possess two equivalent eclipsed B_6 triangles interconnected by three B_2 units on the cage surface and three deca-coordinate La centers in three conjoined η^{10}-B_{10} rings, we manually constructed the perfect tetrahedral cage-like T_d La_4B_{24} (**1**) with four equivalent interconnected B_6 triangles on the cage surface and four nona-coordinate La centers in four conjoined η^9-B_9 rings (Fig.1) Encouragingly, extensive GM searches show that, being overwhelmingly more stable than other low-lying isomers, La_4B_{24} (**1**, $^1A_1$) is the well-defined GM of the neutral (Fig. S1) with the lowest vibrational frequency of υ_{min} = 119.87 cm^{-1} at PBE0. It is 0.79 eV more stable than the second lowest-lying isomer C_s La_4B_{24} with a B_2 core and 1.23 eV more stable than the third lowest-lying isomer C_s La_4B_{24} with a B_3 core at CCSD(T) level, respectively (Fig. S1). The triplet cage-like C_1 La_4B_{24} (^3A) slightly distorted due to Jahn-Teller effect appears to be much less stable than the T_d GM (by 1.28 eV) at PBE0 (Fig. S1). La_4B_{24} (**1**) possesses the B-B bond length of $r_{B–B}$ = 1.57 Å between the interconnected B_6 triangles, B-B bond, length of r'_{B-B} = 1.66 Å within the central B_3 triangles in B_6 triangular motifs, and average La–B coordination bond length of $r_{La–B}$ = 2.75 Å between La atoms and their η^9-B_9 ligands. The large calculated HOMO–LUMO gap of ΔE_{gap} = 2.35 eV at PBE0 well supports its high chemical stability. Cage-like La_4B_{24} (**1**) appears to be the first metallo-borospherene possessing the same tetrahedral symmetry as its

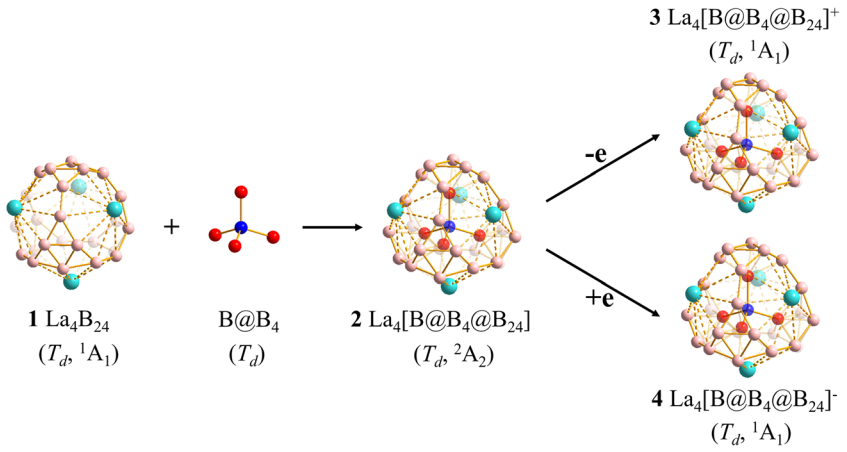

Fig. 1 Optimized structures of cage-like T_d La_4B_{24} (**1**) and core-shell T_d $La_4[B@B_4@B_{24}]$ (**2**), T_d $La_4[B@B_4@B_{24}]^+$ (**3**), and T_d $La_4[B@B_4@B_{24}]^-$ (**4**), with the central B atom highlighted in blue and four apex B atoms of the tetrahedral T_d $B@B_4$ core highlighted in red in **2, 3**, and **4**

carbon fullerene counterpart—the experimentally observed quintet T_d C_{28} ($^5A_1$) [29]. Extensive molecular dynamic simulations indicate that La_4B_{24} (**1**) is also highly dynamically stable, with the small calculated average root-mean-square-deviations of RMSD = 0.13 Å and maximum bond length deviations of MAXD = 0.43 Å at 1000 K, respectively (Fig. 2). Detailed NBO analyses show that the La centers in La_4B_{24} (**1**) possess the natural atomic charge of $q_{La} = +1.49$ |e| and electronic configuration of $La[Xe]4f^{0.16}5d^{1.32}6s^{0.09}$, indicating that La donates its $6s^2$ electron almost completely to the surrounding B_9 ligand in La_4B_{24} (**1**) while accepting partial valence electron (~0.32 |e|) from the boron ligand in its partially occupied 5d orbitals via p → d back donations. Bond order analyses show that the La centers in La_4B_{24} (**1**) possess the total Wiberg bond order of $WBI_{La} = 2.79$ and average La–B bond order of $WBI_{La-B} = 0.26$, evidencing the formation of effective La–B coordination interactions in the complex.

The high-symmetry tetrahedral T_d $La_4[B@B_4@B_{24}]$ (**2**) ($^2A_2$) was achieved by encapsulating a B-centered tetrahedral T_d $B@B_4$ core inside the cage-like La_4B_{24} (**1**), forming a perfect tetrahedral core-shell lanthanide boride complex with a tetra-coordinate B at the cage center (Fig. 1). Surprisingly and intriguingly, extensive DFT calculations indicate that,

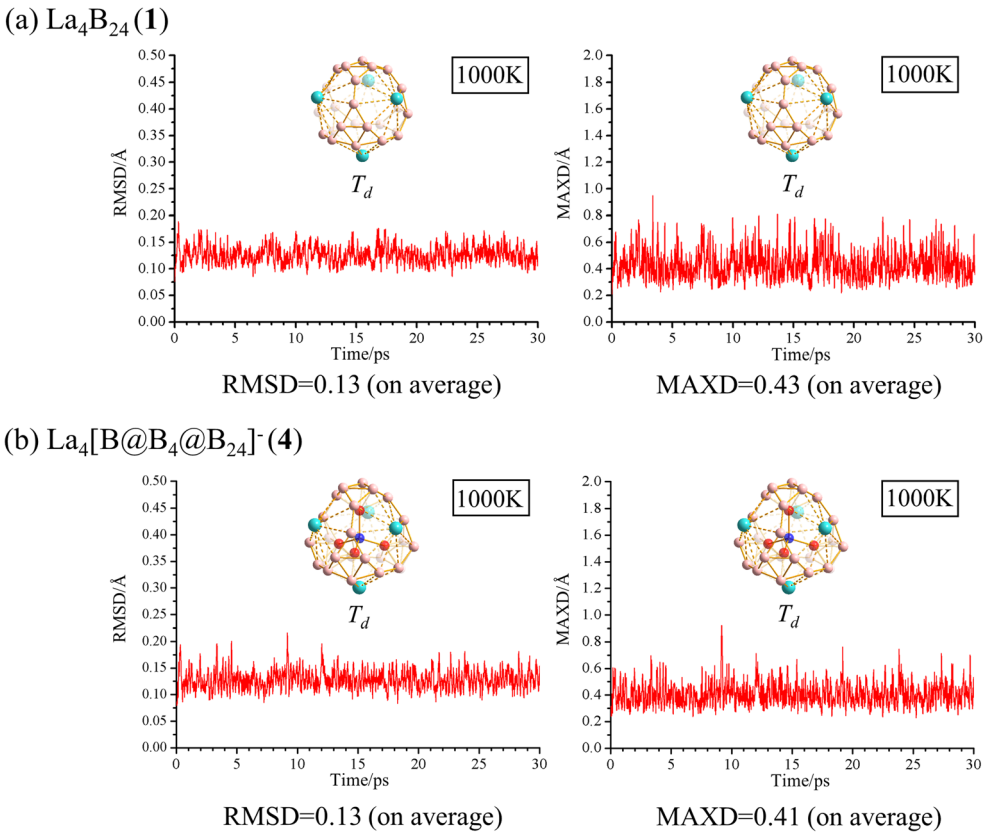

Fig. 2 Born-Oppenheimer molecular dynamics simulations of La_4B_{24} (**1**) (a) and $La_4[B@B_4@B_{24}]^-$ (**4**) (b) at 1000 K. The root-mean-square-deviation (RMSD) and maximum bond length deviation (MAXD) values (on average) are indicated in Å

with a singly occupied non-degenerate highest occupied α-orbital (a_2), the doublet $La_4[B@B_4@B_{24}]$ (**2**) well retains its identical tetrahedral T_d symmetry during full structural optimizations. As the most stable isomer obtained, it lies 0.79 eV lower than the second lowest-lying isomer C_1 La_4B_{29} (^{2}A) (Fig. S2). The tetrahedral $B@B_4$ core and La_4B_{24} (**1**) shell turn out to match both geometrically and electronically in $La_4[B@B_4@B_{24}]$ (**2**) which has the lowest vibrational frequency of $\upsilon_{min} = 128.94$ cm^{-1} and α-HOMO-LUMO gap of $\Delta E_{gap} = 2.23$ eV. Detaching one election from or attaching one electron to $La_4[B@B_4@B_{24}]$ (**2**) results in the perfect singlet T_d $La_4[B@B_4@B_{24}]^+$ (**3**, $^1A_1$) and T_d $La_4[B@B_4@B_{24}]^-$ (**4**, $^1A_1$) which also appear to be the well-defined GMs of the systems lying 0.79 eV and 0.69 eV lower than the second lowest-lying core-shell C_s $La_4B_{29}^+$ and C_1 $La_4B_{29}^-$ at PBE0, respectively (Fig. S3 and Fig. S4). $La_4[B@B_4@B_{24}]^{+/-}$ (**3/4**) possess the large HOMO-LUMO gaps of $\Delta E_{gap} = 2.84/2.21$ eV and lowest vibrational frequencies of $\upsilon_{min} = 125.50/131.35$ cm^{-1}. The $La_4[B@B_4@B_{24}]^{0/+/-}$ (**2/3/4**) core-shell complex series in a 1 + 4 + 28 structural motif possess the B-B bond lengths of $r_{B\text{-}B} = 1.65/1.64/1.66$ Å between the central B atom and inner tetrahedron $(B^i)_4$, B-B distances of $r_{B\text{-}B} = 1.73/1.73/1.73$ Å between the inner tetrahedron $(B^i)_4$ and outer tetrahedron $(B^o)_{24}$, and the La–B distances of $r_{La\text{–}B} = 2.88/2.93/2.85$ Å between the B atom at the center and La atoms on the outer shell. They can thus be viewed as the first bi-shell metallo-borospherenes with the tetrahedral B center encapsulated in an inner tetrahedron $(B^i)_4$ and an outer tetrahedron $La_4(B^o)_{24}$. Similar to the previously reported endohedral metallosilicon fullerenes T_d $M_4@Si_{28}$ (M = Al and Ga) which follow the structural motif of 4 + 28 [28], core-shell $La_4[B@B_4@B_{24}]^{0/+/-}$ (**2/3/4**) in the structural motif of 1 + 4 + 28 possess the same tetrahedral symmetry as their carbon fullerene counterpart T_d C_{28} [29]. These core-shell complexes also appear to be highly dynamically stable, as exemplified in Fig. 2 for $La_4[B@B_4@B_{24}]^-$ (**4**) which has the small calculated average RMSD = 0.13 Å and MAXD = 0.41 Å at 1000 K, respectively.

The behavior of the central B atom in these core-shell complexes appears to be especially interesting. Detailed NBO analyses indicate that the central B in $La_4[B@B_4@B_{24}]^{0/+/-}$ (**2/3/4**) possesses the natural atomic charge of $q_B = -1.00/-1.05/-1.00$ |e|, electronic configurations of $B[He]2s^{0.51}2p^{3.48}/B[He]2s^{0.52}2p^{3.52}/B[He]2s^{0.52}2p^{3.52}$, and total Wiberg bond orders of $WBI_B = 3.71/3.71/3.71$, respectively. The central B atom thus carries approximately a unit negative charge of $q_B \approx -1.0$ |e| in these complexes regardless of the charge states of the systems, resulting in a B^- monoanion at the cage center which is isovalent with a neutral C atom. The negatively charged tetra-coordinate B^- center in **2**, **3**, **4** is thus a boron analog of the tetrahedral C in T_d CH_4, indicating the $B^- \sim C$ analogy [44] in these B-centered core-shell complexes. The tetrahedral T_d $B^-@B_4$ unit in $La_4[B@B_4@B_{24}]^{0/+/-}$ (**2/3/4**) appears to have the same symmetry as the well-known tetrahedral T_d BH_4^- (which is isovalent with T_d CH_4 [44]), in obvious contrast to the experimentally observed planar C_{2v} B_5^- in gas phase [2, 3] due to effective B(p)-B_6(π) σ interactions between the $B^-@B_4$ core and T_d B_{24} outer shell (as detailed below).

Bonding analyses

To better interpret the high stabilities of these T_d lanthanide boride complexes, we performed detailed AdNDP bonding analyses on the closed-shell La_4B_{24} (**1**) and $La_4[B@B_4@B_{24}]^+$ (**3**) to recover both the localized and delocalized bonds of the systems. As shown in Fig. 3(a), La_4B_{24} (**1**) possesses 6 2c-2e B-B σ bonds with the occupation number of ON = 1.88 |e| between the four interconnected B_6 triangles on the cage surface and 16 3c-2e σ bonds with ON = 1.91 |e| on four equivalent B_6 triangular motifs, forming the σ skeleton of the cage-like system. Over the σ skeleton, there exist 4 equivalent 6c–2e π bonds with ON = 1.91 over four quasi-planar B_6 triangles at the corners. The remaining 16 delocalized bonds are mainly responsible for the La–B_9 coordination interactions in the complex, including 12 equivalent 5c-2e La–B_4 (d-p) σ bonds with ON = 1.72 and 4 equivalent 10c-2e La–B_9 (d-p) δ bond with ON = 1.62 evenly distributed over four La@B_9 nonagons on the cage surface. Such a bonding pattern renders spherical aromaticity to cage-like La_4B_{24} (**1**), as evidenced by the calculated negative nucleus-independent chemical shift (NICS) [45] values of NICS = −31.69 ppm at the cage center and NICS = −33.41 ppm 1.0 Å above the cage center along the C_2 molecular axes.

Figure 3(b) indicates that the core-shell $La_4[B@B_4@B_{24}]^+$ (**3**) well inherits the main bonding elements of La_4B_{24} (**1**), with the 6 2c-2e B-B σ bonds, 16 3c-2e σ bonds, 12 5c-2e La–B_4 (d-p) σ bonds, and 4 10c-2e La-B_9 (d-p) δ bonds remaining basically unchanged. The main difference occurs at the 4 2c-2e B-B σ-bonds in the $B@B_4$ core beween the central B atom and $(B^i)_4$ inner tetrahedron and 4 7c-2e B_6(π)-B(p) σ interactions between the four B^i atoms in the inner shell and four capping B_6 triangles in the outer shell in the first row and 3 29c-2e π-p σ bonds totally delocalized on the core-shell B_{29} framework ([$B@B_4@B_{24}$]) in the fourth row. Interestingly, similar to La_4B_{24} (**1**), $La_4[B@B_4@B_{24}]^{0/+/-}$ (**2/3/4**) possess the negative calculated NICS values of NICS = -33.92/−43.18/−28.19 ppm 1.0 Å above the B center along the C_2 molecular axes, respectively, indicating that these core-shell borospherenes are also spherically aromatic in nature. The 12 5c-2e La–B_4 (d-p) σ and 4 10c-2e La–B_9 (d-p) δ coordination bonds in La_4B_{24} (**1**) and $La_4[B@B_4@B_{24}]^+$ (**3**) play a vital role in stabilizing these perfect tetrahedral lanthanide boride complexes.

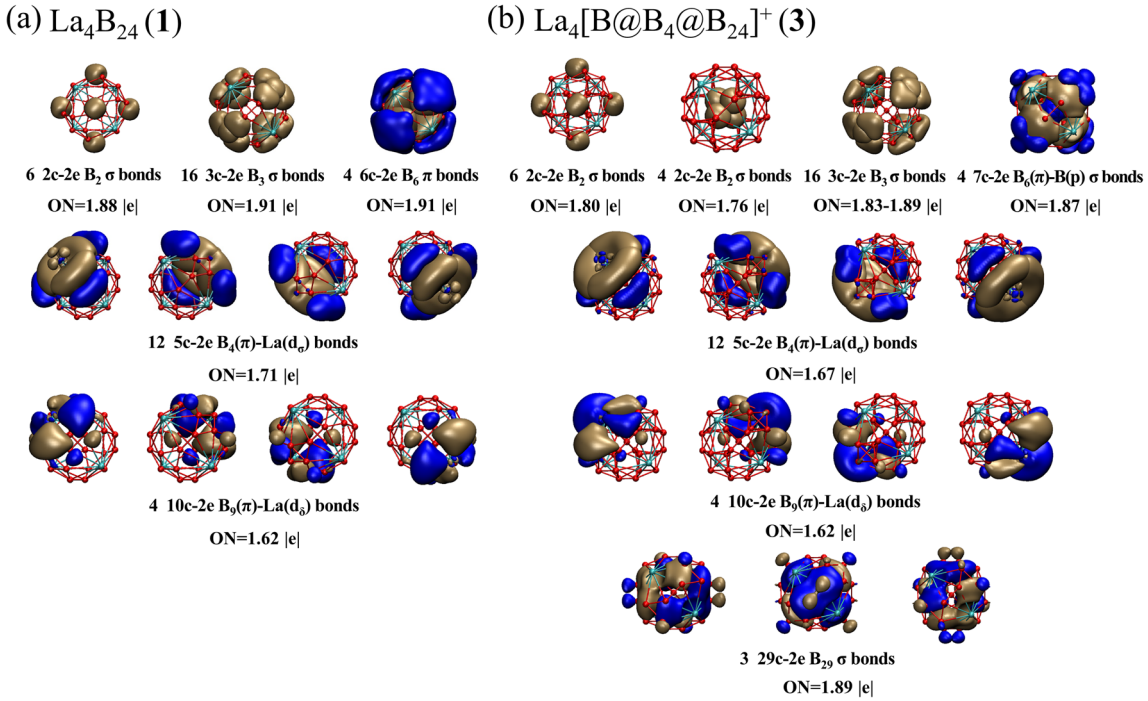

Fig. 3 AdNDP bonding patterns of the closed-shell La_4B_{24} (**1**) (a) and $La_4[B@B_4@B_{24}]^+$ (**3**) (b), with the occupation numbers (ONs) indicated

IR, Raman, and UV-Vis/PES spectral simulations

The IR, Raman, and UV-Vis spectra of La_4B_{24} (**1**) and IR, Raman, and PES spectra of $La_4[B@B_4@B_{24}]^-$ (**4**) are computationally simulated in Fig. 4 to facilitate their future characterizations. T_d La_4B_{24} (**1**) possesses highly simplified IR and Raman spectra due to its high symmetry, including four sharp IR peaks at 215(t_2), 239(t_2), 810(t_2), and 1036 (t_2) cm^{-1} and eight active Raman vibrations at 137 (a_1), 239(t_2), 391(a_1), 473(a_1), 1036(t_2), 1065(a_1), 1257(t_2), and 1267(a_1)

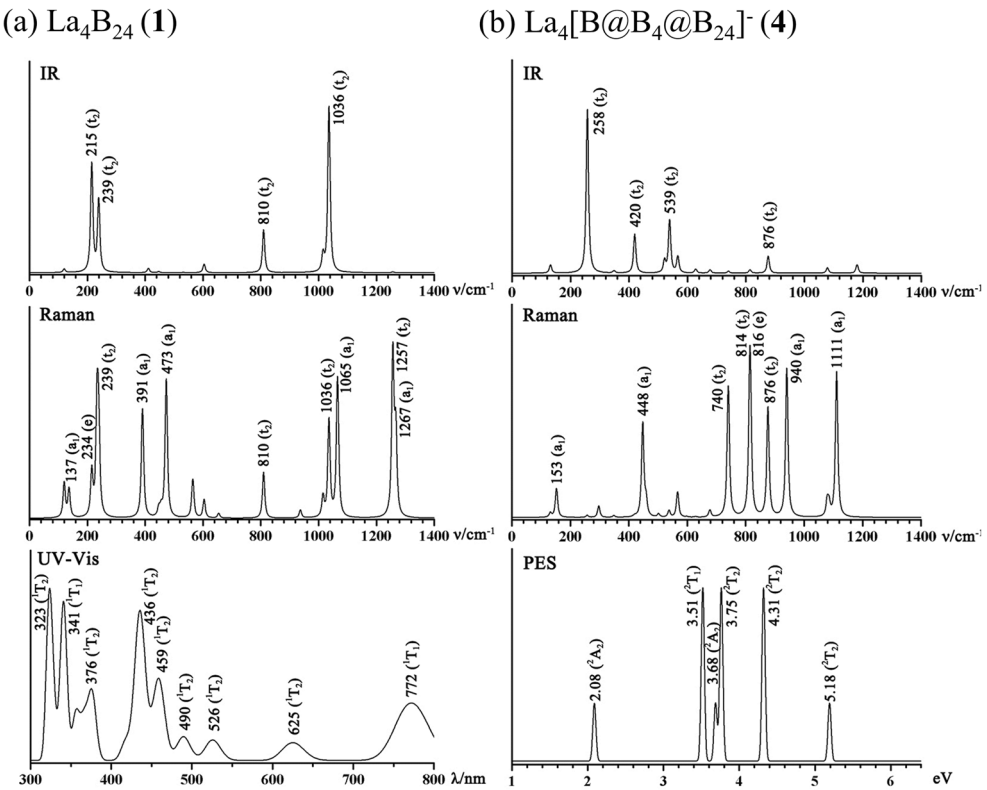

Fig. 4 Simulated IR, Raman, and UV-Vis spectra of La_4B_{24} (**1**) (**a**) and IR, Raman, and PES spectra of $La_4[B@B_4@B_{24}]^-$ (**4**) (**b**) at PBE0 level

cm^{-1}, respectively. Detailed vibrational analyses indicate that the symmetrical vibrations at 137 cm^{-1} (a_1) and 391 cm^{-1} (a_1) represent typical radial breathing modes (RBMs) of the cage-like complex which can be used to characterize single-walled hollow boron nanostructures [46]. The strong UV bands around 323, 341, 376, 436, and 459 nm originate from electronic transitions from deep inner shells of the neutral to its high-lying unoccupied molecular orbitals, while the weak broad bands around 490, 526, 625, and 772 nm mainly involve electronic excitations from the occupied frontier orbitals around the HOMO (t_2) of the neutral. As shown in Fig. 4(b), $La_4[B@B_4@B_{24}]^-$ (**4**) exhibits similar IR and Raman spectral features to La_4B_{24} (**1**), with the strongest IR vibration at 258 cm^{-1} (t_2) and typical RBM vibrations at 153 cm^{-1} (a_1) and 448 (a_1) cm^{-1}. The calculated PES spectrum of $La_4[B@B_4@B_{24}]^-$ (**4**) exhibits major spectral features at 2.08, 3.51, 3.75, 4.31, and 5.18 eV which correspond to vertical electronic transitions from the ground state of the anion ($^1A_1$) to the ground state ($^2A_2$) and excited states ($^2T_1$, $^2T_2$, $^2T_2$, $^2T_2$) of the neutral at the ground-state geometry of the anion, respectively.

Conclusions

Perfect tetrahedral cage-like La_4B_{24} (**1**) and core-shell $La_4B_{29}^{0/+/-}$ (**2**/**3**/**4**) with spherical aromaticity have been predicted in this work at first-principles theory level to be the first metallo-borospherenes reported to date possessing the same tetrahedral symmetry as their carbon fullerene counterpart T_d C_{28}. The tetrahedral $B@B_4$ core and tetrahedral La_4B_{24} (**1**) shell match both geometrically and electronically in the $La_4B_{29}^{0/+/-}$ (**2**/**3**/**4**) series. Such species could be synthesized and characterized in gas phases using a La-B binary target in PES experiments. [21–24] These high-symmetry lanthanide boride complexes and their chemically modified derivatives may serve as building blocks to form various nanoclusters and nanomaterials with novel electronic, magnetic, and optical properties.

Supplementary Information The online version of this article (https://doi.org/10.1007/s00894-021-04739-8) contains supplementary material, which is available to authorized users.

Availability of data and material All the data are available online.

Code availability N/A

Authors' contributions Z. H. Wei and S. D. Li designed the project and X. Q. Lu and C. Y. Gao performed the calculations. All the authors participate in the discussion and preparation of the manuscript.

Funding The work was supported by the National Natural Science Foundation of China (21720102006 and 21973057 to S.-D. Li).

Declarations

Conflict of interest The authors declare no conflicts of interests.

References

1. Cotton FA, Wilkinson G, Murrillo CA, Bochmann M, *Advanced Inorganic Chemistry*, Wiley, New York, 6th edn, 1999, p. 1355, ISBN 0-471-19957-5
2. Wang LS (2016) Photoelectron spectroscopy of size-selected boron clusters: from planar structures to borophenes and borospherenes. Int. Rev. Phys. Chem. 35:69–142. https://doi.org/10.1080/0144235X.2016.1147816
3. Jian T, Chen XN, Li SD, Boldyrev AI, Li J, Wang LS (2019) Probing the structures and bonding of size-selected boron and doped-boron clusters. Chem. Soc. Rev. 48:3550–3591. https://doi.org/10.1039/c9cs00233b
4. Chen Q, Li WL, Zhao YF, Zhang SY, Hu HS, Bai H, Li HR, Tian WJ, Lu HG, Zhai HJ, Li SD, Li J, Wang LS (2015) Experimental and theoretical evidence of an axially chiral Borospherene. ACS Nano 9:754–760. https://doi.org/10.1021/nn506262c
5. Zhai HJ, Zhao YF, Li WL, Chen Q, Bai H, Hu HS, Piazza ZA, Tian WJ, Lu HG, Wu YB, Mu YW, Wei GF, Liu ZP, Li J, Li SD, Wang LS (2014) Observation of an all-boron fullerene. Nat. Chem. 6:727–731. https://doi.org/10.1038/nchem.1999
6. Bai H, Chen TT, Chen Q, Zhao XY, Zhang YY, Chen WJ, Li WL, Cheung LF, Bai B, Cavanagh J, Huang W, Li SD, Li J, Wang LS (2019) Planar B_{41}^- and B_{42}^- clusters with double-hexagonal vacancies. Nanoscale 11:23286–23295. https://doi.org/10.1039/C9NR09522E
7. Wang YJ, Zhao YF, Li WL, Jian T, Chen Q, You XR, Ou T, Zhao XY, Zhai HJ, Li SD, Li J, Wang LS (2016) Observation and characterization of the smallest borospherene, B_{28}^- and B_{28}. J. Chem. Phys. 144:064307. https://doi.org/10.1063/1.4941380
8. Li HR, Jian T, Li WL, Miao CQ, Wang YJ, Chen Q, Luo XM, Wang K, Zhai HJ, Li SD, Wang LS (2016) Competition between quasi-planar and cage-like structures in the B_{29} cluster: photoelectron spectroscopy and ab initio calculations. Phys. Chem. Chem. Phys. 18:29147–29155. https://doi.org/10.1039/C6CP05420J
9. Bai H, Chen Q, Zhai HJ, Li SD (2015) Endohedral and Exohedral Metalloborospherenes: $M@B_{40}$ (M=Ca, Sr) and $M\&B_{40}$ (M=Be, Mg). Angew. Chem. Int. Ed. 54:941–945. https://doi.org/10.1002/anie.201408738
10. Li HR, Liu H, Tian XX, Zan WY, Mu YW, Lu HG, Li J, Wang YK, Li SD (2017) Structural transition in metal-centered boron clusters: from tubular molecular rotors $Ta@B_{21}$ and $Ta@B_{22}^+$ to cage-like endohedral metalloborospherene $Ta@B_{22}^-$. Phys. Chem. Chem. Phys. 19:27025–27030. https://doi.org/10.1039/C7CP05179D
11. Yu TR, Gao Y, Xu DX, Wang ZG (2018) Actinide endohedral boron clusters: a closed-shell electronic structure of $U@B_{40}$. Nano Res. 11:354. https://doi.org/10.1007/s12274-017-1637-9
12. Oger E, Crawford NRM, Kelting R, Weis P, Kappes MM, Ahlrichs R (2007) Boron cluster Cations: transition from planar to cylindrical structures. Angew. Chem. Int. Ed. 46:8503–8506. https://doi.org/10.1002/anie.200701915
13. Sai LW, Wu X, Gao N, Zhao JJ, King RB (2017) Boron clusters with 46, 48, and 50 atoms: competition among the core–shell, bilayer and quasi-planar structures. Nanoscale 9:13905–13909. https://doi.org/10.1039/C7NR02399E
14. Pei L, Ma YY, Yan M, Zhang M, Yuan RN, Chen Q, Zan WY, Mu YW, Li SD (2020) Bilayer B_{54}, B_{60}, and B_{62} clusters in a universal structural pattern. Eur. J. Inorg. Chem. 34:3296–3301. https://doi.org/10.1002/ejic.202000473

15. Romanescu C, Galeev TR, Li WL, Boldyrev AI, Wang LS (2011) Aromatic metal-centered monocyclic boron rings: Co©B_8^- and Ru©B_9^-. Angew. Chem. Int. Ed. 50:9334–9337. https://doi.org/10.1002/ange.201104166
16. Galeev TR, Romanescu C, Li WL, Wang LS, Boldyrev AI (2012) Observation of the highest coordination number in planar species: Decacoordinated Ta©B_{10}^- and Nb©B_{10}^- anions. Angew. Chem. Int. Ed. 51:2101–2105. https://doi.org/10.1002/ange.201107880
17. Jian T, Li WL, Popov IA, Lopez GV, Chen X, Boldyrev AI, Li J, Wang LS (2016) Manganese-centered tubular boron cluster – MnB_{16}^-: a new class of transition-metal molecules. J. Chem. Phys. 144:154310. https://doi.org/10.1063/1.4946796
18. Popov IA, Jian T, Lopez GV, Boldyrev AI, Wang LS (2015) Cobalt-centred boron molecular drums with the highest coordination number in the CoB_{16}^- cluster. Nat. Commun. 6:8654. https://doi.org/10.1038/ncomms9654
19. Jian T, Li WL, Chen X, Chen TT, Lopez GV, Li J, Wang LS (2016) Competition between drum and quasi-planar structures in RhB_{18}^-: motifs for metallo-boronanotubes and metallo-borophenes. Chem. Sci. 7:7020–7027. https://doi.org/10.1039/C6SC02623K
20. Li WL, Jian T, Chen X, Li HR, Chen TT, Luo XM, Li SD, Li J, Wang LS (2017) Observation of a metal-centered B_2-Ta@B_{18}^- tubular molecular rotor and a perfect Ta@B_{20}^- boron drum with the record coordination number of twenty. Chem. Commun. 53:1587–1590. https://doi.org/10.1039/C6CC09570D
21. Li WL, Chen TT, Xing DH, Chen X, Li J, Wang LS (2018) Observation of highly stable and symmetric lanthanide octa-boron inverse sandwich complexes. Proc. Natl. Acad. Sci. U. S. A. 115:E6972–E6977. https://doi.org/10.1073/pnas.1806476115
22. Chen TT, Li WL, Li J, Wang LS (2019) $[La(\eta^x\text{-}B_x)La]^-$ (x = 7–9): a new class of inverse sandwich complexes. Chem. Sci. 10:2534–2542. https://doi.org/10.1039/c8sc05443f
23. Chen TT, Li WL, Chen WJ, Li J, Wang LS (2019) $La_3B_{14}^-$: an inverse triple-decker lanthanide boron cluster. Chem. Commun. 55:7864–7867. https://doi.org/10.1039/c9cc03807h
24. Chen TT, Li WL, Chen WJ, Yu XH, Dong XR, Li J, Wang LS (2020) Spherical trihedral metallo-borospherenes. Nat. Commun. 11:2766. https://doi.org/10.1038/s41467-020-16532-x
25. Lu XQ, Chen Q, Tian XX, Mu YW, Lu HG, Li SD (2019) Predicting lanthanide boride inverse sandwich tubular molecular rotors with the smallest core–shell structure. Nanoscale 11:21311–21316. https://doi.org/10.1039/c9nr07284e
26. Zhao XY, Yan M, Wei ZH, Li SD (2020) Donor–acceptor duality of the transition-metal-like B_2 core in core–shell-like metallo-borospherenes La_3&$[B_2@B_{17}]^-$ and La_3&$[B_2@B_{18}]^-$. RSC Adv. 10:34225–34230. https://doi.org/10.1039/d0ra06769e
27. Zhang Y, Zhao XY, Yan M, Li SD (2020) From inverse sandwich $Ta_2B_7^+$ and Ta_2B_8 to spherical trihedral $Ta_3B_{12}^-$: prediction of the smallest metallo-borospherene. RSC Adv. 10:29320–29325. https://doi.org/10.1039/d0ra05570k
28. Gao Y, Zeng XC (2005) M_4@Si_{28} (M=Al, Ga): metal-encapsulated tetrahedral silicon fullerene. J. Chem. Phys. 123:204325. https://doi.org/10.1063/1.2121568
29. Guo T, Diener Chai M, Alford MJ, Haufler RE, McClure SM, Ohno T, Weaver JH, Scuseria GE, Smalley RE (1992) Science Uranium Stabilization of C_{28} : A Tetravalent Fullerene. 257:1661–1664. https://doi.org/10.1126/science.257.5077.1661
30. Chen X, Zhao YF, Zhang YY, Li J (2019) TGMin: an efficient global minimum searching program for free and surface-supported clusters. J. Comput. Chem. 40:1105–1112. https://doi.org/10.1002/jcc.25649
31. Adamo C, Barone V (1999) Toward reliable density functional methods without adjustable parameters: the PBE0 model. J. Chem. Phys. 110:6158–6170. https://doi.org/10.1063/1.478522
32. Tao J, Perdew JP, Staroverov VN, Scuseria GE (2003) Climbing the density functional ladder: non-empirical meta-generalized gradient approximation designed for molecules and solids. Phys. Rev. Lett. 91:146401. https://doi.org/10.1103/PhysRevLett.91.146401
33. Krishnan R, Binkley JS, Seeger R, Pople JA (1980) Self-consistent molecular orbital methods. XX. A basis set for correlated wave functions. J Chem Phys 72: 650. https://doi.org/10.1063/1.438955
34. Feller D (1996) The role of databases in support of computational chemistry calculations. J. Comput. Chem. 17:1571–1586. https://doi.org/10.1002/(SICI)1096-987X
35. Schuchardt L, Didier B, Elsethagen T, Sun L, Gurumoorthi V, Chase J, Li J, Windus TL (2007) Basis set exchange: a community database for computational sciences. J. Chem. Inf. Model. 47:1045–1052. https://doi.org/10.1021/ci600510j
36. Frisch MJ, Trucks GW, Schlegel HB, Scuseria GE, Robb MA, Cheeseman JR, Scalmani G, Barone V, Mennucci B, Petersson GA et al (2009) Gaussian 09, revision D.01. Gaussian, Inc., Wallingford
37. Čížek J (1969) On the use of the cluster expansion and the technique of diagrams in calculations of correlation effects in atoms and molecules. Adv. Chem. Phys. 14:35–89. https://doi.org/10.1002/9780470143599.ch2
38. Purvis III GD, Bartlett RJ (1982) A full coupled-cluster singles and doubles model: the inclusion of disconnected triples. J. Chem. Phys. 76:1910. https://doi.org/10.1063/1.443164
39. Raghavachari K, Trucks GW, Pople JA, Head-Gordon M (1989) A fifth-order perturbation comparison of electron correlation theories. Chem Phys Lett 157: 479-483. Https:// doi.org/157.1989/479
40. Werner HJ, et al., Molpro, version 2012.1
41. Tkachenko NV, Boldyrev AI (2019) Chemical bonding analysis of excited states using the adaptive natural density partitioning method. Phys. Chem. Chem. Phys. 21:9590–9596. https://doi.org/10.1039/c9cp00379g
42. Glendening PED, Badenhoop JK, Reed AE, Carpenter JE, Bohmann JA, Morales CM, Landis CR, Weinhold F. NBO 6.0, 2013
43. VandeVondele J, Krack M, Mohamed F, Parrinello M, Chassaing T, Hutter J (2005) QUICKSTEP: fast and accurate density functional calculations using a mixed Gaussian and plane waves approach. Comput. Phys. Commun. 167:103–128. https://doi.org/10.1016/j.cpc.2004.12.014
44. Alexandrova AN, Birch KA, Boldyrev AI (2003) Flattening the $B_6H_6^{2-}$ octahedron Ab initio prediction of a new family of planar all-boron aromatic molecules. J. Am. Chem. Soc. 125:10786–10787. https://doi.org/10.1021/ja0361906
45. Schleyer PR, Maerker C (1996) Nucleus-independent chemical shifts: a simple and efficient Aromaticity probe. J. Am. Chem. Soc. 118:6317–6318. https://doi.org/10.1021/JA960582D
46. Ciuparu D, Klie R, Zhu YM, Pfefferle L (2004) Synthesis of pure boron Single-Wall nanotubes. J. Phys. Chem. B 108:3967–3969. https://doi.org/10.1021/jp049301b